J Appl Electrochem (2016) 46:851–860
DOI 10.1007/s10800-016-0961-1

RESEARCH ARTICLE

Carbon nanotubes cross-linked Zn_2SnO_4 nanoparticles/graphene networks as high capacities, long life anode materials for lithium ion batteries

Hui Shan[1,2,3] · Yang Zhao[1,2,4] · Xifei Li[1,2] · Dongbin Xiong[1,2] · Lei Dong[1,2] · Bo Yan[1,2] · Dejun Li[1,2] · Xueliang Sun[1,2,4]

Received: 1 March 2016 / Accepted: 16 April 2016 / Published online: 29 April 2016

Abstract By shielding zinc stannate (ZTO, viz., Zn_2SnO_4) nanoparticles with reduced graphene oxide (RGO) as well as multi-wall carbon nanotubes (MWCNTs), we have successfully created ZTO/RGO/MWCNTs composites via a facile hydrothermal process. In the designed hybrid nanostructure, acting as the strut and bridge to open the graphene sheets, 3D RGO/MWCNT nets not only tackle the problem of volume expansion and the aggregation of ZTO nanoparticles, but also maintain the integration of anode materials for high electrochemical performance. As a result, the resultant anode material shows high reversible capacity, superior rate capacity and long-running cycle performance for lithium ion batteries (LIBs). For instance, a excellent reversible capacity of 915.9 mAh g^{-1} was obtained at the current density of 100 mA g^{-1} after 340 cycles. Our study demonstrates significant potential of ZTO/RGO/MWCNTs as anode materials for LIBs.

Graphical Abstract

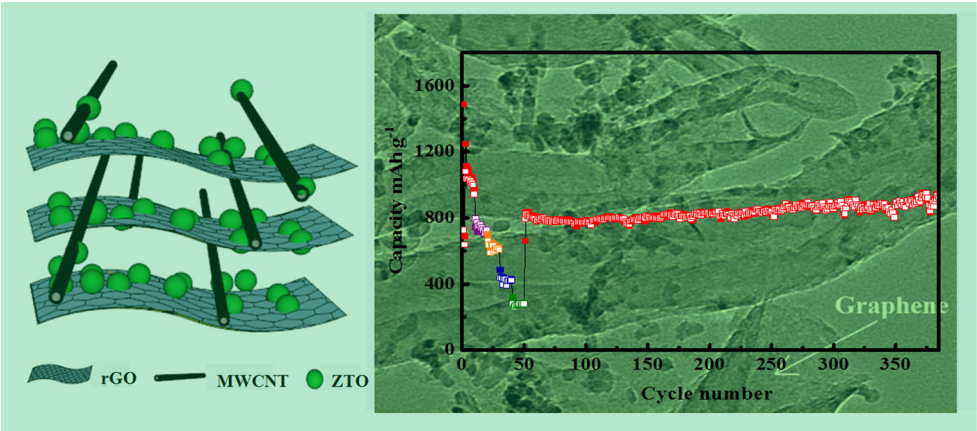

Hui Shan and Yang Zhao these authors have contributed equally.

✉ Xifei Li
xfli2011@hotmail.com

✉ Dejun Li
dejunli@mail.tjnu.edu.cn

✉ Xueliang Sun
xsun@eng.uwo.ca

[1] Energy & Materials Engineering Centre, College of Physics and Materials Science, Tianjin Normal University, Tianjin 300387, China

[2] Tianjin International Joint Research Centre of Surface Technology for Energy Storage Materials, Tianjin 300387, China

Keywords Zn_2SnO_4 nanoparticles · Reduced graphene oxide · Carbon nanotubes · Lithium ion batteries · Anode materials

1 Introduction

As one of the most popular commercial energy storage devices, lithium-ion batteries (LIBs) attract huge attention in both industries and academe due to their large-scale applications [1–3]. The increasing requirements of power rate, cycle lifetime, and safety make it urgent to find a substitute for traditional graphite anode materials in LIBs. At full lithiation, graphitic carbon can only reveal a limited capacity of 372 mAh g^{-1} [4, 5]. Therefore, numerous practical operations have been directed to the development of new electrode materials with superior reversible capacities. Due to the high natural abundance and theoretical capacities [6] (>600 mAh g^{-1}), metal oxides (Co_3O_4 [7] , Mn_2O_3 [8], ZnO [9], SnO_2 [10], NiO [11], et al.) are supposed to be the possible anode candidates for high-performance LIBs. By contrast, tin-based materials attracted considerable attention with the high theoretical specific capacity but relatively low working potentials. Moreover, by the introduction of transition elements Zn, the working potentials and energy densities of tin-based materials can be effectively controlled. For example, Zn_2SnO_4 (ZTO) possesses unique properties of high theoretical irreversible capacity of 1231 mAh g^{-1}, superior electron mobility of 10–15 $cm^2v^{-1}s^{-1}$ and a wide band gap of 3.6 eV. However, the inevitable restriction of pulverization disadvantage resulting from the high volume changes has been still a bottleneck during the alloying reactions with lithium. Consequently, a lot of efforts have been contributed to stabilizing the structures of anode materials as well as engineering the interfaces with electrolyte. For instance, nano-crystallized materials, nanotubes, hollow spheres and nestlike nanospheres were already widely reported [12–14]. Other conventional methods of volume change control consist of surface chemistry modification, coating modification, and so on.

Reportedly, there are various extrinsic designs of hybrid structures applied in the electrode for LIB anodes. Wang et al. proposed SnO_2@CNT with a reversible capacity of 880 mAh g^{-1} after 200 cycles at 100 mA g^{-1}, where monodispersed SnO_2 nanoparticles existed within 3D connected carbon networks, by dexterously utilizing the porous structures and adsorption properties of MOFs [15]. Zhong et al. proposed a two-stage calcination process to successfully synthesize Sn@graphene-based nanosheets incorporating of optimized nitrogen species, and this anode delivered the discharge capacity of 890 mAh g^{-1} after continuous tests from 0.1 to 1 A^{-1} cycle at 100 mA g^{-1} [16]. By contrast, our strategy to design a ZTO/GRO/MWCNTs nanocomposite via a facile hydrothermal process with primary calcination is more inexpensive and tunable as well as much easier to perform, more importantly, the superior performance 915.9 mAh g^{-1} after 340 cycles at 100 mA g^{-1} was achieved. Therefore, on the basis of highly-efficient electron conductivity and flexible and robust mechanical properties, carbon allotropes, such as graphene and carbon nanotubes were focused on the composite design with proper incorporation to further strengthen the Li storage performance [17]. Graphene, as an excellent carbonaceous material, was reported to mitigate aforementioned obstacles due to its essential virtue, such as large surface area, high mechanical strength, strong chemical stability and superior electrical conductivity [18, 19]. As for the composites of metal oxide/RGO, the subdued volume change and improved electrical conductivity efficiently facilitate the electron transport rate and maintain the integration of the electrodes in LIBs. For instance, a SnO_2–graphene nanocomposite exhibited a higher capacity of 520 mAh g^{-1} compared with the SnO_2 nanoparticles failing completely after 100 cycles [20]. The RGO/C/ZnO anode materials exhibited the reversible capacity of 600 mAh g^{-1} after 50 cycles, and this value was far more than bare ZnO aggregates [21]. Another type of $CoMoO_4$/rGO composite revealed the better cycling performance (628 mAh g^{-1} in the 100th cycle) than $CoMoO_4$ electrodes with only 321 mAh g^{-1} [22]. However, it is inevitable to prevent the forming of solid-electrolyte-interphase (SEI) film on the surface of anode in the initial stage and the aggregation due to the π–π stacking interaction in the later drying process of graphene. Therefore, some researchers reported that the incorporation of carbon nanotubes (CNT) can physically separate the graphene nanosheets, and alleviate these problems in certain extent in LIB utilization. For example, graphene–MWCNT reveals a specific capacity of 768 mAh g^{-1} at the current density of 100 mA g^{-1} after 100 cycles, which is 2.5 times superior to that of pure graphene [23]. TiO_2/RGO/CNT was demonstrated to exhibit the capacity loss of 8.7 % after 100 cycles, less than that of TiO_2/RGO (11.5 %) and pristine TiO_2 (14.7 %) [2]. It was found that without adding CNT, Ge/RGO maintains a specific capacity of 863.8 mAh g^{-1} after 100 cycles at the current density of 100 mA g^{-1}, but exhibits a inferior cycle life performance compared with Ge/RGO/CNT [24].

[3] National Key Laboratory of Power Sources, Tianjin Institute of Power Sources, Tianjin 300381, China

[4] Nanomaterials and Energy Lab, Department of Mechanical and Materials Engineering, University of Western Ontario, London, ON N6A 5B9, Canada

In this work, we construct a novel nanocomposite featuring carbon nanotubes cross-linked Zn_2SnO_4 nanoparticles/graphene network. It not only favors the electrolyte ion and electron transfer, but also prompts the closer contact area between the electrolyte and electrode. More importantly, RGO and CNT play a vital role to tackle some handicaps including the volume expansion as well as the aggregation of ZTO nanoparticles. As a result, it is believed that the anode nanocomposite shows enhanced electrochemical performance for LIBs.

2 Experimental

2.1 Materials Synthesis

The graphene oxide was obtained by a modified Hummers' method, which has been previously reported by our group [25, 26]. In a typical experiment, GO dispersion (3 mg mL^{-1}) was obtained by ultrasonic of the resultant dry graphite oxide powder in deionized water for 30 min. Then the desirable dispersion was centrifuged for 30 min (10000 r/min) to wipe out some aggregates, afterwards repeating sonicating the GO aqueous dispersion with extraneous MWCNTs. Subsequently, $Zn(CH_3COO)_2{\cdot}2H_2O$ and $SnCl_4{\cdot}5H_2O$ with the mole ratio: 2: 1 were added into the solution, diethanol amine, 1,2-propanediol and GO solution (3 mg/mL) with volume ratio of 1: 2: 2, under vigorous stirring for 30 min, and the as-prepared dispersions were transferred to a Teflon-lined autoclave (50 mL) and maintained at 200 °C for 24 h. Then the as-obtained product was filtered and washed with ethanol and deionized water for several times, and freeze-dried overnight. Finally, the resultant materials were calcined at 600 °C for 3 h under an argon atmosphere labeled as ZTO/RGO/MWCNTs. For comparison, the product without MWCNTs or only $Zn(CH_3COO)_2{\cdot}2H_2O$ and $SnCl_4{\cdot}5H_2O$ was synthesized under the same conditions, which was labeled as ZTO/RGO and ZTO, respectively.

2.2 Materials characterization

The powder XRD patterns of the products were recorded with an X-ray diffractometer (Germany, D8 Advance of Bruker) using Cu/K_α radiation between 5^o and 85^o. The FT-IR spectra were obtained on an IRAffinity-1 FT-IR spectrometer (Shimadzu), and the samples were prepared for FT-IR measurement by grinding the KBr dried powder with and compressing into the pellets. The morphologies of the samples were verified using field-emission scanning electron microscopy (FE-SEM, Hitachi, SU8010) as well as high-resolution transmission electron microscopy (HR-TEM, JEM-3000F).

2.3 Electrochemical characterization

The lithium storage performance of as-obtained samples was investigated utilizing CR2032 coin-type cells. The manufacture of working electrode was prepared via mixing active material, acetylene black (Super-P) and polyvinylidenefluoride (PVDF) binder according to the ratio of 7.5:1.5:1 in *N*-methyl-2-pyrrolidinone (NMP). Then the mixture was subsequently coated on the copper foil following the dry process in vacuums at 90 °C for 12 h. The coin cells assembled in a glove box filling with purity argon, employing pure lithium as counter electrode and reference electrode, 1 M $LiPF_6$ was added in a solution containing dimethyl carbonate and ethylene carbonate as electrolyte. Cyclic voltammograms (CV) were tested using an electrochemical workstation (Princeton Applied Research Versa STAT 4) at a scan rate of 0.1 mV s^{-1} within the voltage range of 0.01–3.0 V (vs. Li/Li^+). The electrode performance was symbolized by the galvanostatic discharge–charge curves in a voltage range from 0.01 to 3.0 V (vs. Li/Li^+) with the battery testing system (LANHE CT2001A). The data of the electrochemical impedance spectroscopy (EIS) was obtained by Princeton Applied Research (Versa STAT 4) at a frequency from 0.01 Hz to 100 kHz.

3 Results and discussion

Scheme 1 depicts the synthesis process of ZTO/RGO/MWCNTs network nanocomposite. The oxidation exfoliation of graphite produces graphite oxide through the modified Hummers' method. First, ultrasonic treatment benefits to uniformly mix GO and MWCNTs, and a cross-linked appearance with the individual interacted MWCNTs adsorbed onto the GO surface by p-stacking is observed. Then, a certain amount of $Zn(CH_3COO)_2{\cdot}2H_2O$ and $SnCl_4{\cdot}5H_2O$ was added into the GO/MWCNTs suspension and mixed equally. Finally, the products were fabricated via one-step hydrothermal reaction combined with sequent thermal treatment. Delightedly, the cross-linked structure consisting of ZTO, RGO and MWCNTs was expected to exhibit enhanced performance.

The XRD patterns of ZTO/RGO and ZTO/RGO/MWCNTs clarifying the phase purity and crystallographic structure were shown in Fig. 1a. Perfectly assigned to the ideal cubic inverse spinel, the standard data (PDF#24-1470) indexed by the correlative diffraction peaks indicates high pure ZTO. The lattice planes of (111), (220), (311), (222), (400), (422), (511), (440) and (533) are located at 17.7°, 29.1°, 34.2°, 35.9°, 41.6°, 51.6°, 55.0°, 60.4° and 71.3° respectively. The (002) peak of ZTO/RGO/MWCNTs is not observed in ZTO/RGO, which may be due to the deposition of MWCNTs on the surface of graphene.

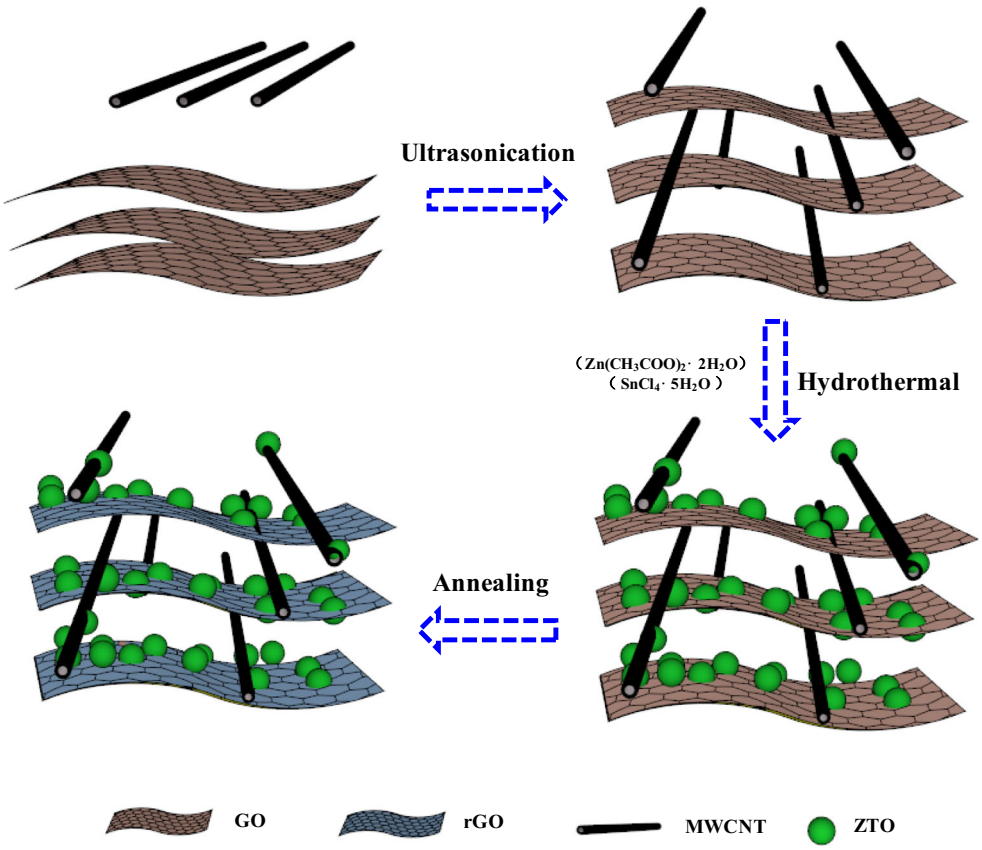

Scheme 1 Schematic illustration of the preparation process of ZTO/RGO/MWCNTs nanocomposite

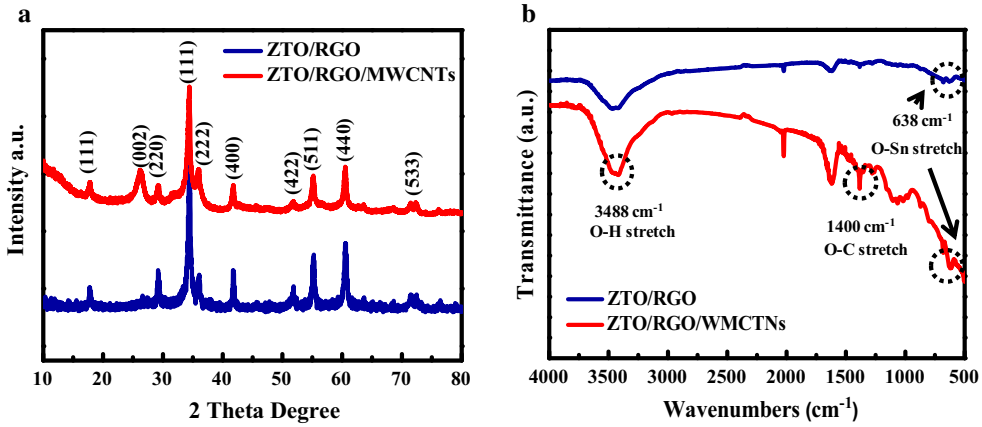

Fig. 1 **a** XRD patterns; and **b** FTIR spectra of ZTO/RGO and ZTO/RGO/MWCNTs

To evaluate the interactions between C-, O-, Zn- and Sn- during the synthetic process of ZTO/RGO and ZTO/RGO/MWCNTs, FT-IR spectra were measured within the range of 4000–500 cm^{-1}, as revealed in Fig. 1b. The absorption peaks are related to chemical composition and crystalline structure. As previously reported [27], the bands located at 3488, 1400 and 6387 cm^{-1} are the regions of remarkableness, corresponding to the stretching vibration of H–O, O–C and O–Sn, respectively. These results prove a composite of ZTO/RGO/MWCNTs rather than $ZnSn(OH)_6$ and other heterostructures symbolized by the Sn–O–H and $[Sn(OH)_6]^{2-}$ etc. [28]. Additionally, the oxygen-containing functional groups in the graphene and CNT surface were found.

Figure 2a, b shows SEM images of ZTO/RGO/MWCNTs at high and low magnifications. It can be identified that the nanocomposites were wrapped around by graphene with the typical rippled and crumpled structure, as well as MWCNTs with longer length uniformly dispersed in the surface of RGO [25]. More importantly, in

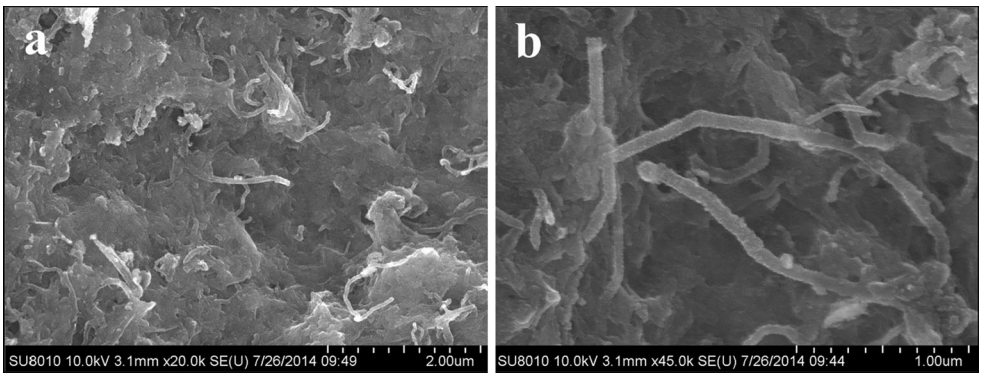

Fig. 2 Typical SEM images of ZTO/RGO/MWCNTs

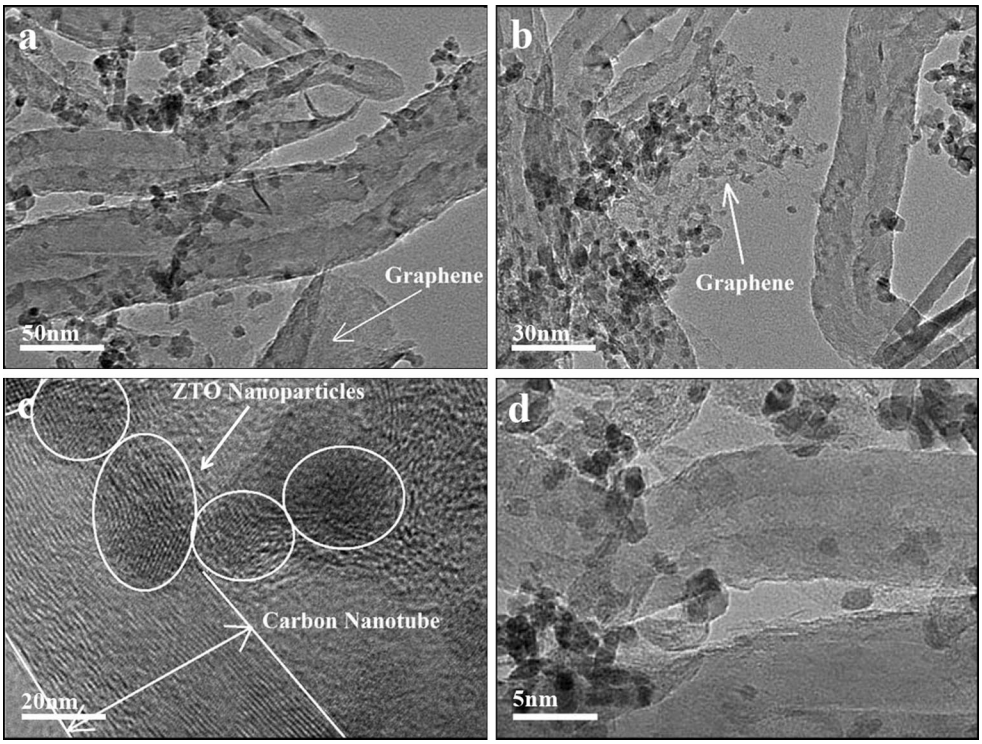

Fig. 3 **a**, **b**, **c** TEM and **d** HRTEM images of ZTO/RGO/MWCNTs

Fig. 2b, ZTO nanoparticles were routinely anchored on CNT and graphene layers. In this design, MWCNTs were used as the strut and bridge to open the graphene sheets, which avoids agglomerating with each other, and facilitates the diffusion of lithium ion and electrons. Moreover, graphene was utilized as the substrate materials for the deposit of ZTO nanoparticles. This unique structure can mitigate the particle-fracture in electrode materials, and thus slow capacity fade of the anode materials for lithium-ion batteries.

TEM and HR-TEM images were shown in Fig. 3 to further investigate the morphology of carbon nanotubes cross-linked Zn_2SnO_4 nanoparticles loading on graphene network. The lattice fringe of about 0.306 nm corresponds to the (220) plane of ZTO. From the architecture of the composite assembled by the uniformly distributed ZTO nanoparticles attaching on the MWCNTs and graphene surface, one can verify the successful incorporation of our product rather than several individuals.

Figure 4a compares the cycling performance of ZTO nanoparticles, ZTO/RGO and ZTO/RGO/MWCNTs electrodes at a current density of 100 mA g^{-1}. It can be found that in the initial cycle, high discharge capacities of ZTO nanoparticles (1678.6 mAh g^{-1}), ZTO/RGO (1499.6 mAh g^{-1}) and ZTO/RGO/MWCNTs (1507.6 mAh g^{-1}) were obtained. Clearly, the three samples delivered various

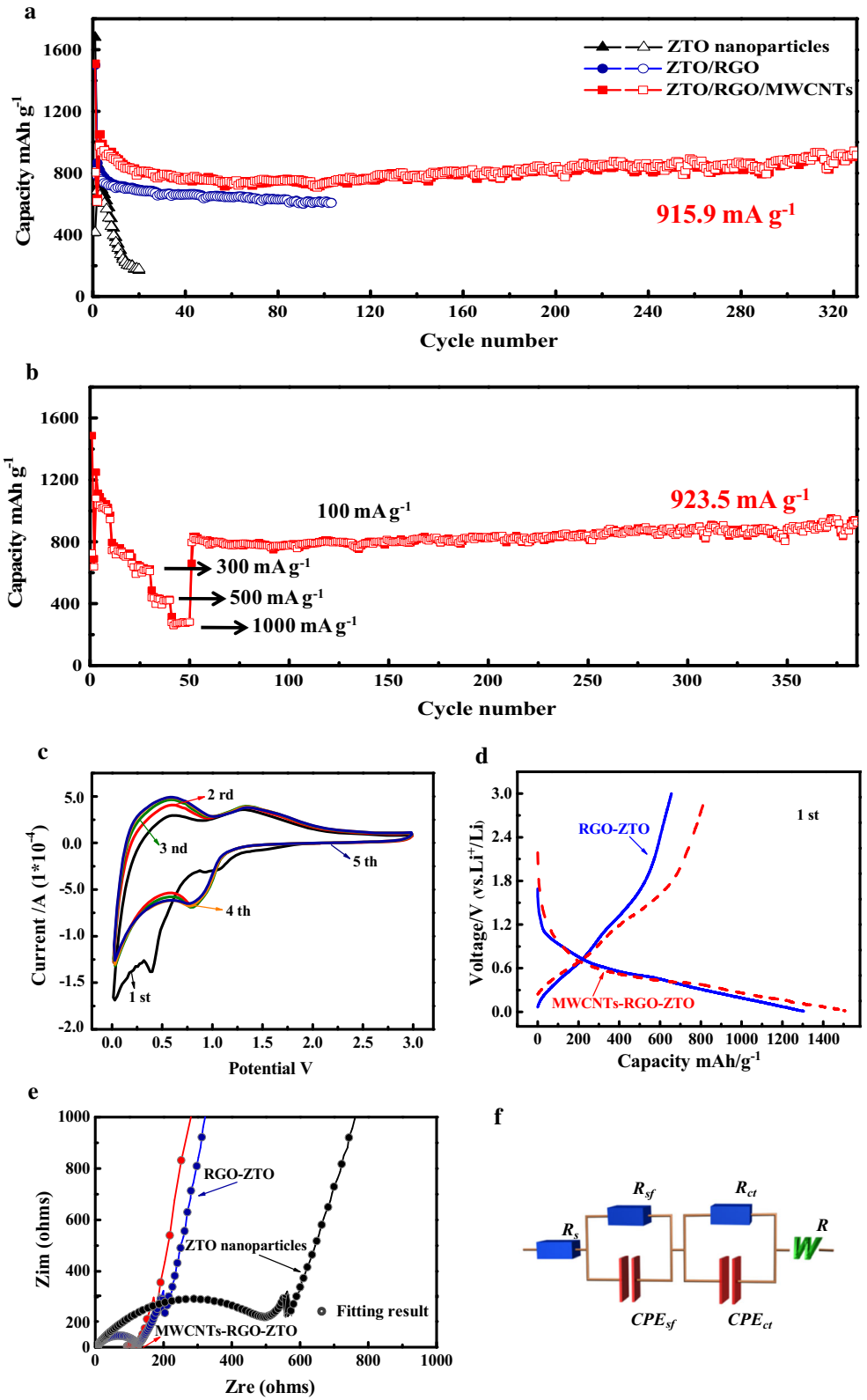

Fig. 4 **a** The comparison of cycling performance of ZTO nanoparticles, ZTO/RGO and ZTO/RGO/MWCNTs at a current density of 100 mA g^{-1}; **b** Rate performance of ZTO/RGO/MWCNTs at various current densities; **c** Cyclic voltammograms of ZTO/RGO/MWCNTs in the voltage range of 0.01–3 V (vs. Li/Li^+) at a scanning rate of 0.2 mV s^{-1}; **d** Discharge/charge voltage profiles of the ZTO/RGO and ZTO/RGO/MWCNTs for the first cycle; **e** Nyquist plots of ZTO nanoparticles, ZTO/RGO and ZTO/RGO/MWCNTs; **f** The equivalent circuit used to simulate an experimental curve

cyclability upon cycling. The ZTO nanoparticles anode shows the worst performance with a low discharge capacity of 167.8 mAh g^{-1} within 20 cycles. It is widely documented that this poor performance may be related to the irreversible formation of Li_2O matrix and the active interreaction between the compounds of Li–Sn and Li–Zn [26–31], as well as the pulverization problem and the sustainable consumption of lithium-ion by the breaking and reforming of solid electrolyte interphase (SEI) films. Take advantages of RGO, the ZTO/RGO anode shows a specific discharge capacity of 608.6 mAh g^{-1} at the 100th cycle benefiting from the 3D conductive graphene network. After introduction of MWCNTs, capacity fading of the anode material was further greatly alleviated, for instance, it revealed a super reversible capacity of up to 915.9 mAh g^{-1} after 330 cycles. The main reasons of the capacity improvement may be ascribed to the functions of the acceptable electronic conduct, high specific surface area and the specific porous structure [32].

Figure 4b shows the rate performances of ZTO/RGO/MWCNT anode at the varied current density range of 100–1000 mA g^{-1}. The specific capacities reduced progressively as the current density increased, but the anode worked stably at each current density. It is noteworthy that at the highest current density of up to 1000 mA g^{-1}, a reversible capacity of 283.8 mAh g^{-1} was still obtained. When the current density returns to 100 mA g^{-1}, it retains a discharge capacity of 923.5 mAh g^{-1} in the 385th cycle, which demonstrated the significant function of the capability of the ZTO/RGO/MWCNTs electrodes with long life cycle. The superior rate properties ought to be attributed to the synergetic effects deriving from ZTO, graphene and MWCNTs which build the efficient connections in the novel 3D conductive network to protect the integrity of electrode material.

To identify the electrochemical reactions in the initial five cycles, cyclic voltammetry (CV) was conducted at ambient temperature at a scan rate of 0.1 mV s^{-1} in the voltage ranging from 0.01 to 3.0 V, as shown in Fig. 4c. Based on the electrochemical process of ZTO/RGO/MWCNTs, a proposed Li storage mechanism is listed as follows [33]:

$$4Li^+ + Zn_2SnO_4 + 4e^- \rightarrow Sn + 2Li_2O + 2ZnO \quad (1)$$

$$8Li^+ + Zn_2SnO_4 + 8e^- \rightarrow 2Zn + Sn + 4Li_2O \quad (2)$$

$$xLi^+ + Sn + xe^- \leftrightarrow Li_xSn \ (0 \le x \le 4.4) \quad (3)$$

$$yLi^+ + Zn + ye^- \leftrightarrow Li_xZn \ (0 \le x \le 4.4) \quad (4)$$

It can be found that, with Li metal used as the counter electrode, an intensive reduction peak located at 0.39 V disappears in the following cycles. It corresponds to the forming of SEI films on the electrode surface as well as the decomposition of the electrolyte. The evident cathodic peak appearing at 0.8 V and the anodic peaks at 1.25 and 0.56 V in the first cycle match with the process of multi-step lithium insertion reaction (Eqs. 1 and 2), which elaborates the irreversible reduction of Zn_2SnO_4 to Sn or Zn generating the amorphous Li_2O and delithiation respectively. In the subsequent anodic scan, the extended peaks occur at 0.30 and 0.60 V as well as the anodic peaks at 0.55 and 1.5 V correspond to certain reversible reactions and the de-alloying process of Li_yZn and Li_xSn (Eqs. 3 and 4).

The electrochemical performance of the as-prepared ZTO/RGO and ZTO/RGO/MWCNTs was evaluated by galvanostatic discharge/charge testing at a current density of 100 mA g^{-1}. As shown in Fig. 4d, the capacities of ZTO/RGO in the first discharge and charge cycles are 1304.06 and 655.91 mAh g^{-1} respectively, while the introduction of MWCNTs increases both values, that is, 1507.6 and 828.84 mAh g^{-1}, respectively. Notably, the ZTO/RGO/MWCNTs electrode shows higher capacity, and delivers a higher coulombic efficiency (54.97 %) over ZTO/RGO electrode (50.30 %). These results highlight the synergistic effect of the novel nanocomposite featuring carbon nanotubes cross-linked Zn_2SnO_4 nanoparticles/graphene network.

The electrochemical impedance spectroscopy (EIS) was certified the improved electrical conductivity of ZTO/RGO/MWCNTs (see the Nyquist plots in Fig. 4e). By fitting the Nyquist plots via the equivalent circuit (Fig. 4f), the impedance data were analyzed accurately. The circuit include ohmic resistance (R_s), two RC parallel elements in series demonstrating the SEI film on the surface (R_{sf} and CPE_{sf}), lithium ion charge transfer at interface (R_{ct} and CPE_{ct}), and Warburg impedance for solid state diffusion of lithium ions. A constant phase element (CPE) was used in the equivalent circuit instead of a pure capacitance due to the inhomogeneous surface of the thin film working electrode. CPE_{sf} and CPE_{ct} are constant phase elements corresponding to the surface film and double layer capacitance, respectively. According to the fitting results presented in Table 1, ZTO/RGO shows a lower charge transfer resistance (110.9 Ω) than ZTO nanoparticles (411.6 Ω). By adding the MWCNTs, the ZTO/RGO/

Table 1 The typical fitted parameters in the electrochemical impedance spectroscopy

Samples	R_{sf}	R_{ct}	CPE_{sf}	CPE_{ct}
ZTO	0.68	411.6	7.79E−06	4.54E−05
ZTO/RGO	1.33	110.9	1.08E−05	1.50E−05
ZTO/RGO/CNTs	1.2E−03	25.45	0.03	2.03E−05

Table 2 Comparison of the electrochemical performance of the ZTO materials reported before and in this work

Materials	Synthesis method	Electrochemical performance			Ref
		Current density (mA g^{-1})	Cycle number	Capacity retention (mAh g^{-1})	
MWCNTs-RGO-ZTO	Hydrothermal method	100	325	915	This work
Co–ZTO–G–C	Hydrothermal method	100	50	699	[35]
Mn_3O_4/ZTO	Hydrothermal method	100	50	577.4	[36]
ZTO boxes@C/graphene	Multi-step reaction	300	50	726.9	[37]
ZTO boxes/graphene	Co-precipitation method	300	45	752.9	[38]
Graphene wrapped ZTO boxes	Electrostatic interaction	300	45	678.2	[39]
N–C/ZTO Boxes	Co-precipitation method	300	45	616	[40]
Hollow ZTO Boxes	Co-precipitation method	300	45	540	[41]
ZTO Octahedron	Hydrothermal method	50	20	642.2	[42]
ZTO Nanospheres	Hydrothermal Method	100	60	602	[43]

MWCNTs network with the superior conductivity delivers the much smaller value of 0.0012 Ω for R_{sf} and 25.45 Ω for R_{ct} respectively which is favorable for the transport of Li ions and the access of electrolyte as well as prompts in the optimized electrochemical performance [9, 34].

Table 2 shows the comparison of the electrochemical performance of the ZTO materials previously reported and in this work. A series of researches were reported. The original strategy is to design different novel nano/micro structure of ZTO with relative stable structure and high surface area, such as hollow box, octahedron or nanospheres. However, the low electrical conductive and large volume change highly affect the performances of ZTO. As a result, numerous additives with flexible structure and high electrical conductive, such as graphene, N-doped carbon and conductive polymer, have been introduced to synthesize the composites with ZTO. Moreover, multi-structure of ZTO composites have been developed with two or more types of conductive and buffering matrix, like the Co–ZTO–G–C and ZTO boxes@C/graphene. In this study, we design a novel kind of RGO and MWCNTs coexisted with ZTO nanocomposites. Compared with the previous results (Table 2), the ZTO nanocomposites with MWCNTs and cross-linked RGO network improve the electrochemical performance, and it opens a new strategy to develop tin-based based materials for LIBs.

4 Conclusion

In summary, we have developed a novel ZTO/RGO/MWCNTs architectures by anchoring ZTO nanoparticles on the surface of intertwined MWCNTs and wrinkled graphene, to form an advanced electrode materials for LIBs. The microstructures, compositions and electrochemical performance of the abtained product were investigated in detail. The results reveal that the introduction of GO and MWCNTs effectively alleviate the capacity fading and optimize the ZTO electrodes with considerable electronic conduct, high specific surface area and novel porous structure. It is trustworthy that the designed carbon nanotubes cross-linked Zn_2SnO_4 nanoparticles/graphene network holds great promise as durable anode materials in LIBs.

Acknowledgments This research was supported by the National Natural Science Foundation of China (51572194), the Key Projects of Tianjin Municipal Natural Science Foundation of China (14JCZDJC32200), LPMT, CAEP (KF14006), Academic Innovation Funding of Tianjin Normal University (52XC1404), Scientific Research Foundation for Returned Overseas Chinese Scholars of State Education Ministry, Training Plan of Leader Talent of University in Tianjin and the program of Thousand Youth Talents in Tianjin of China. XS and YZ thanks support from the Natural Science and Engineering Research Council of Canada and the Canada Research Chair Program.

References

1. Wang X, Li G, Hassan FM, Li M, Feng K, Xiao X et al (2015) Building sponge-like robust architectures of CNT–graphene–Si composites with enhanced rate and cycling performance for lithium-ion batteries. J Mater Chem A 3:3962–3967
2. Shen L, Zhang X, Li H, Yuan C, Cao G (2011) Design and tailoring of a three-dimensional TiO_2–graphene–carbon nanotube nanocomposite for fast lithium storage. J Phys Chem Lett 2:3096–3101
3. Byon HR, Gallant BM, Lee SW, Shao-Horn Y (2013) Role of oxygen functional groups in carbon nanotube/graphene free-standing electrodes for high performance lithium batteries. Adv Funct Mater 23:1037–1045
4. Huang B, Yang J, Zou Y, Ma L, Zhou X (2014) Sonochemical synthesis of SnO_2/carbon nanotubes encapsulated in graphene

sheets composites for lithium ion batteries with superior electrochemical performance. Electrochim Acta 143:63–69
5. Zhang B, Zheng QB, Huang ZD, Oh SW, Kim JK (2011) SnO_2–graphene–carbon nanotube mixture for anode material with improved rate capacities. Carbon 49:4524–4534
6. Su Y, Li S, Wu D, Zhang F, Liang H, Gao P, Cheng C, Feng X (2012) Two-Dimensional carbon-coated graphene/metal oxide hybrids for enhanced lithium storage. ACS Nano 6:8349–8356
7. Huang G, Xu S, Lu S, Li L, Sun H (2014) Micro-/nanostructured Co_3O_4 anode with enhanced rate capability for lithium-ion batteries. ACS Appl Mater Interfaces 6:7236–7243
8. Su H, Xu YF, Feng SC, Wu ZG, Sun XP, Shen CH et al (2015) Hierarchical Mn_2O_3 hollow microspheres as anode material of lithium ion battery and its conversion reaction mechanism investigated by XANES. ACS Appl Mater Interfaces 7:8488–8494
9. Köse H, Karaal Ş, Aydın AO, Akbulut H (2015) A facile synthesis of zinc oxide/multiwalled carbon nanotube nanocomposite lithium ion battery anodes by sol–gel method. J Power Sources 295:235–245
10. Zhou X, Wan LJ, Guo YG (2013) Binding SnO_2 nanocrystals in nitrogen-doped graphene sheets as anode materials for lithium-ion batteries. Adv Mater 25:2152–2157
11. Yan B, Li M, Li X, Bai Z, Dong L, Li D (2015) Electrochemical impedance spectroscopy illuminating performance evolution of porous core-shell structured nickel/nickel oxide anode materials. Electrochim Acta 164:55–61
12. Park M, Kim M, Joo J, Kim K, Kim J, Ahn S, Cui Y, Cho J (2009) Silicon nanotube battery anodes. Nano lett 9:3844–3847
13. Ma H, Cheng F, Chen JY, Zhao JZ, Li CS, Tao ZL et al (2007) Nest-like silicon nanospheres for high-capacity lithium storage. Adv Mater 19:4067–4070
14. Yao Y, McDowell MT, Ryu I, Wu H, Liu N, Hu L et al (2011) Interconnected silicon hollow nanospheres for lithium-ion battery anodes with long cycle life. Nano Lett 11:2949–2954
15. Wang M, Yang H, Zhou X, Shi W, Zhou Z, Cheng P (2015) Rational design of SnO_2@C nanocomposites for lithium ion batteries by utilizing adsorption properties of MOFs. Chem Commun (Camb) 52:717–720
16. Zhong Y, Yang M, Zhou X, Zhou Z (2015) Structural design for anodes of lithium-ion batteries: emerging horizons from materials to electrodes. Mater Horiz 2:553–566
17. Zhong Y, Yang M, Zhou X, Wei J, Zhou Z (2015) Towards excellent anodes for Li-ion batteries with high capacity and super long lifespan: confining Ultrasmall Sn particles into N-Rich graphene-based nanosheets. Part Part Syst Char 32:104–111
18. Chen S, Yeoh W, Liu Q, Wang G (2012) Chemical-free synthesis of grap hene carbon nanotube hybrid materials for reversible lithium storage in lithium-ion batteries. Carbon 50:4557–4565
19. Zhong C, Wang J-Z, Wexler D, Liu H-K (2014) Microwave autoclave synthesized multi-layer graphene/single-walled carbon nanotube composites for free-standing lithium-ion battery anodes. Carbon 66:637–645
20. Yao J, Shen X, Wang B, Liu H, Wang G (2009) In situ chemical synthesis of SnO_2–graphene nanocomposite as anode materials for lithium-ion batteries. Electrochem Commun 11:1849–1852
21. Wi S, Woo H, Lee S, Kang J, Kim J, An S et al (2015) Reduced graphene oxide/carbon double-coated 3-D porous ZnO aggregates as high-performance Li-ion anode materials. Nanoscale Res Lett 10:204
22. Yang T, Zhang H, luo Y, Mei L, Guo D, Li Q et al (2015) Enhanced electrochemical performance of $CoMoO_4$ nanorods/reduced graphene oxide as anode material for lithium-ion batteries. Electrochim Acta 158:327–332
23. Vinayan BP, Nagar R, Raman V, Rajalakshmi N, Dhathathreyan KS, Ramaprabhu S (2012) Synthesis of graphene-multiwalled carbon nanotubes hybrid nanostructure by strengthened electrostatic interaction and its lithium ion battery application. J Mater Chem 22:9949
24. Fang S, Shen L, Zheng H, Zhang X (2015) Ge–graphene–carbon nanotube composite anode for high performance lithium-ion batteries. J Mater Chem A 3:1498–1503
25. Xiong D, Li X, Shan H, Yan B, Dong L, Cao Y et al (2015) Controllable oxygenic functional groups of metal-free cathodes for high performance lithium ion batteries. J Mater Chem A 3:11376–11386
26. Xiong D, Li X, Shan H, Zhao Y, Dong L, Xu H et al (2015) Oxygen-containing functional groups enhancing electrochemical performance of porous reduced graphene oxide cathode in lithium ion batteries. Electrochim Acta 174:762–769
27. Bhabu KA, Theerthagiri J, Madhavan J, Balu T, Rajasekaran TR (2015) Synthesis and characterization of zinc stannate nanomaterials by Sol-Gel method. Mater Sci Forum 832:144–157
28. Zhang H, Song P, Han D, Yan H, Yang Z, Wang Q (2015) Controllable synthesis of novel $ZnSn(OH)_6$ hollow polyhedral structures with superior ethanol gas-sensing performance. Sensor Actuat B 209:384–390
29. Zhou X, Liu W, Yu X, Liu Y, Fang Y, Klankowski S et al (2014) Tin dioxide@carbon core-shell nanoarchitectures anchored on wrinkled graphene for ultrafast and stable lithium storage. ACS Appl Mater Interfaces 6:7434–7443
30. Ren Y, Zhang J, Liu Y, Li H, Wei H, Li B et al (2012) Synthesis and superior anode performances of TiO_2-carbon-rGO composites in lithium-ion batteries. ACS Appl Mater Interfaces 4:4776–4780
31. Wang X, Cao X, Bourgeois L, Guan H, Chen S, Zhong Y et al (2015) N-Doped graphene-SnO_2 sandwich paper for high-performance lithium-ion batteries. Adv Funct Mater 22:2682–2690
32. Chen M, Liu J, Chao D, Wang J, Yin J, Lin J et al (2014) Porous α-Fe_2O_3 nanorods supported on carbon nanotubes-graphene foam as superior anode for lithium ion batteries. Nano Energy 9:364–372
33. Yuan WS, Tian YW, Liu GQ (2010) Synthesis and electrochemical properties of pure phase Zn_2SnO_4 and composite Zn_2SnO_4/C. J Alloy Compd 506:683–687
34. Yan B, Li X, Bai Z, Li M, Dong L, Xiong D et al (2015) Superior lithium storage performance of hierarchical porous vanadium pentoxide nanofibers for lithium ion battery cathodes. J Alloy Compd 634:50–57
35. Wang H, Wang B, Meng J, Wang J, Jiang Q (2015) One-step synthesis of Co-doped Zn_2SnO_4–graphene–carbon nanocomposites with improved lithium storage performances. J Mater Chem A 3:1023
36. Zhang R, He Y, Li A, Xu L (2014) Facile synthesis of one-dimensional Mn_3O_4/Zn_2SnO_4 hybrid composites and their high performance as anodes for LIBs. Nanoscale 6:14221–14226
37. Huang H, Huang Y, Wang M, Chen X, Zhao Y, Wang K et al (2014) Preparation of hollow Zn_2SnO_4 boxes@C/graphene ternary composites with a triple buffering structure and their electrochemical performance for lithium-ion batteries. Electrochim Acta 147:201–208
38. Zhao Y, Huang Y, Zhang W, Wang Q, Wang K, Zong M et al (2013) Botryoidalis hollow Zn_2SnO_4 boxes@graphene as anode materials for advanced lithium-ion batteries. RSC Adv 3:23489
39. Zhao Y, Huang Y, Sun X, Huang H, Wang K, Zong M et al (2014) Hollow Zn_2SnO_4 boxes wrapped with flexible graphene as anode materials for lithium batteries. Electrochim Acta 120:128–132
40. Zhao Y, Huang Y, Wang Q, Wang K, Zong M, Wang L et al (2014) Hollow Zn_2SnO_4 boxes coated with N-doped carbon for advanced lithium-ion batteries. Ceram Int 40:2275–2280
41. Zhao Y, Huang Y, Wang Q, Wang K, Zong M, Wang L et al (2013) Preparation of hollow Zn_2SnO_4 boxes for advanced lithium-ion batteries. RSC Adv 3:14480

42. Fan H, Liu Z, Yang J, Wei C, Zhang J, Wu L, Zheng W (2014) Surfactant-free synthesis of Zn_2SnO_4 octahedron decorated with nanoplates and its application in rechargeable lithium ion batteries. RSC Adv 4:49806

43. Zhang R, He Y, Xu L (2014) Controllable synthesis of hierarchical $ZnSn(OH)_6$ and Zn_2SnO_4 hollow nanospheres and their applications as anodes for lithium ion batteries. J Mater Chem A 2:17979